FORMATION OF CARBON BUILD-UP ON THE FLUE WALL OF ANODE BAKING FURNACE

Zhaohui Wang[12], Stein Rørvik[1], Arne Petter Ratvik[1] and Tor Grande[2]
[1]SINTEF Materials and Chemistry, NO-7465 Trondheim, Norway
[2]Department of Materials Science and Engineering, Norwegian University of Science and Technology, NO-7491 Trondheim, Norway
Corresponding author: zhaohui.wang@sintef.no, Tel: +47 46249405

Keywords: Carbon build-up, anode baking furnace, pyrolytic carbon

Abstract

A hard carbon build-up layer often forms on the flue wall surface in anode baking furnaces. The layer accumulates over thermal circles and needs to be mechanically removed regularly to ensure sufficient space for the anodes between flue walls. The underlying mechanisms are still unknown and the extent of the carbon build-up varies from plant to plant. The build-up on the flue wall, taken from an autopsy of an open top furnace, has been examined. Microstructure and phase compositions of the carbon build-up, especially towards the refractory interface, were studied by optical microscopy, X-ray computed tomography (CT), SEM/EDS, and XRD. Pyrolytic carbon was found to be the main part of the carbon build-up layer in addition to packing coke particles. The transport of silicon from the refractory material, condensating on the flue wall surface, is found as nucleation sites for the formation of carbon build-up. Formation mechanisms of the carbon build-up are proposed with reaction schemes supported by thermodynamic calculations.

1. Introduction

Reducing the maintenance cost and/or expanding the lift span of refractories in anode backing furnace is one way to reduce the cost of aluminium metal production. Carbon anodes used in aluminium electrolysis can vary in composition, but are normally made from around 70 % petroleum coke, 15-20 % butts, and 14-15 % coal tar pitch as a binder. The green anodes need to be baked before they can be used in aluminium metal production. Volatiles will be released mainly from the pitch during heat treatment of the green anodes. The soaking temperature in the baking furnace is between 1200 °C and 1250 °C. The refractories of the flue walls are subjected to chemical attack, mainly from gaseous species, mechanical impact and large temperature gradients resulting from the thermal cycles. The refractories degrade overtime, especially the surface facing the packing coke towards the anode pits [1-5]. In addition to the mineralogical phase transition of the refractory materials, a hard carbon build-up layer often forms on the flue wall surface in anode baking furnaces. The layer accumulates over thermal cycles and regularly needs to be removed mechanically to ensure sufficient space for the anodes between flue walls. The underlying mechanisms of the carbon build-up formation are still not properly understood, and the extent of the carbon build-up varies from plant to plant.

The carbon build-up on the flue wall, collected during an autopsy of an open top furnace, was studied in this work. The investigation was focused on the microstructure evolution and phase transformation through the build-up layer and at the refractory interface. The formation mechanisms and the corresponding reaction schemes were revealed and supported by thermodynamic calculations using FactSage [6].

2. Autopsies of spent flue wall

Refractory bricks together with carbon build-up layer were collected from a spent flue wall during an autopsy of an open baking furnace with a lifetime of about 4000 days. The carbon build-up layer was around 1-2 cm in thickness. Samples, including the interface between the refractory and the carbon build-up layer, were collected to investigate microstructure evolution and mineralogical phase transformation taking place at the interface. Cross-section samples and powder samples were prepared for characterisation. A piece of carbon build-up layer and a polished interface cross-section sample are shown in Figure 1. A thin black carbon build-up layer could be observed at the refractory interface. Figure 1 also illustrates a schematic drawing partly showing an open top furnace structure including the hollow refractory flue wall, the packing coke and the anode, which are relevant for the present work. The sampling positions are marked in the drawing. Pristine packing coke particles were collected for comparison.

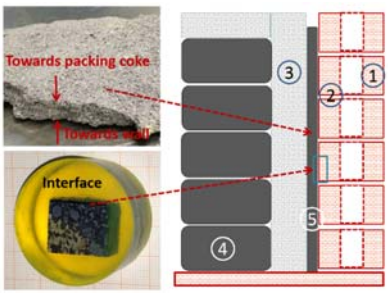

Figure 1. Carbon build-up sample (left top), interface sample (left bottom), and a schematic drawing (right) partly showing an open anode baking furnace structure which is relevant to the present work. 1 - hollow flue wall bricks, 2 - gaps in flue walls to exhaust the volatiles, 3 – packing coke, 4 – green anodes, and 5 – carbon build-up on flue wall surface. Figure only for illustration and not in scale.

Microstructure and phase analysis has been performed on the carbon build-up cross-section and at the refractory interface by scanning electron microscopy (SEM) using LV-SEM HITACHI S-3400N equipped with an energy dispersive spectrometer (EDS) (Hitachi, Japan). Samples with fractured surfaces were also used for a better view of the morphology of each phase. Carbon structure was investigated using optical microscopy with polarizing filter (POL MET) (REICHERT MeF3A). Powder X-ray diffraction (XRD) was performed to detect the main phases in carbon build-up by using a Bruker D8 Focus diffractometer with a LynxEye PSD detector (Bruker AXS, Karlsruhe, Germany).

Non-destructive X-Ray Computed Tomography (CT) was used to inspect the 3-dimensional interior microstructure of the refractory and the carbon build-up, including the interface, using a Nikon XT H225 ST X-ray CT scanner (Nikon Metrology, UK). A tungsten reflection target was used without any filtering. Acceleration voltage was 140 kV with a current of 130 µm, and the image acquisition was done with an integration time of 2000 milliseconds and 3142 projections (π x 1000) per revolution. A cylindrical sample (1 cm in diameter and 1 cm in height) was used for the CT scan. The scanned volume is 2000x2000x2000 voxels, with a voxel size of 5.5 µm in all three directions.

2.1 Carbon build-up layer

The carbon build-up layer was first investigated by SEM/EDS. 2 a) shows the electron image of carbon build-up cross-section, where a coke particle is labelled as number 1 and a white spot is labelled as number 3 while the layered structures growing outwards from the surface of the coke particle and the white spot is labelled as number 2. Figure 2 b) shows the electron image of carbon build-up sample with a fracture surface, where the vivid laminar phase are demonstrated. EDS analysis confirmed that the laminar phase was carbon and the white spots were silica with a minor Na content.

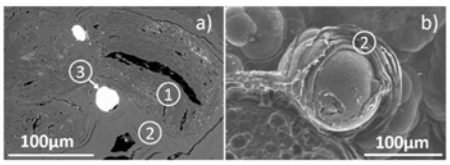

Figure 2. SEM images of carbon build-up. a) cross-section, and b) fracture surface. 1. packing coke particle; 2. layered carbon structure growing on top of the coke particle and white spots; 3. white silica spots

Polarized optical microscope was used to investigate the laminar carbon phase. The polarized light micrographs are presented in Figure 3, where a) shows the spherical laminar structure growing into free space, and b) shows colourful ribbons surrounding coke particles. The laminar carbon phases have crystallised in a planar order. Cleavage planes are clearly shown in the figures. This high-textured carbon phase is pyrolytic carbon [7, 8]. The rough Maltese-cross imply the pyrolytic carbon formed in carbon build-up layer was "rough laminar pyrocarbon" with very anisotropic properties.

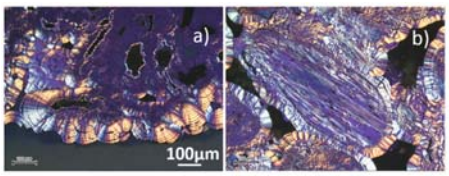

Figure 3. Polarized light micrographs of cross-section of carbon build-up. a) spherical laminar structure with cleavage planes, and b) Ribbon-like structure surrounding a needle coke particle. The two figures have the same magnification

The thickness of the pyrolytic carbon layers varied along the carbon build-up cross-section. Thicker layers around 100 µm were observed near the flue wall surface as presented in Figure 4 a)-b), while slightly into the packing coke the layers were thinner and less than 10 µm as shown in Figure 4 c)-d). Micro-cracks inside the pyrolytic carbon crystals along the cleavage plane are clearly visible in Figure 4 b).

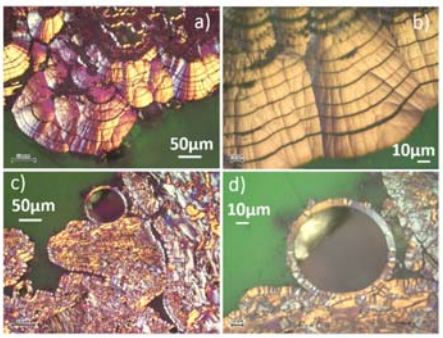

Figure 4. Polarized light micrographs of cross-section of carbon build-up. a) – b) position towards flue wall, and c) - d) position towards packing coke

The main phases detected by powder XRD in the carbon build-up layer were graphite and cristobalite, which was in agreement with SEM/EDS results. XRD diffractograms are shown in Figure 5. Pristine packing coke is also shown for comparison. The splitting of the C_{002} peak is pronounced compared to pristine coke, which is due to the presence of pyrolytic carbon with higher crystallinity.

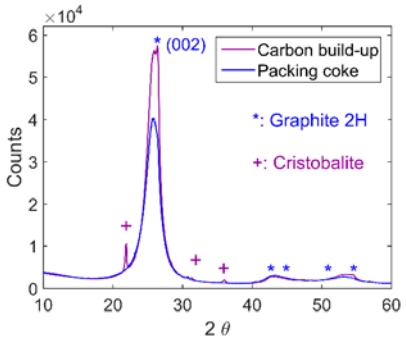

Figure 5. XRD diffractograms for carbon build-up and pristine packing coke

2.2 Refractory interface

The polarized light micrographs of the refractory interface are presented in Figure 6. The refractory material is purple due to the low reflectivity under polarized light. The figure clearly demonstrates that the pyrolytic carbon nucleated on the refractory surface and grew outwards. Several distinct layers could be observed which probably resulted from several thermal cycles. The pyrolytic carbon also infiltrated into the refractory through pores and deposited on the pore surface. The

infiltration depth varied and was in the average of several hundred μm in this sample. The carbon infiltration phenomenon has been confirmed by Loss of Ignition (LOI) test and reported elsewhere [5].

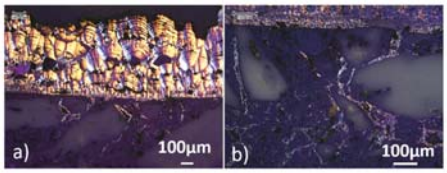

Figure 6. Polarized light micrographs of cross-section of carbon build-up and refractory interface

The dark areas embedded in pyrolytic carbon crystals shown in Figure 6 correspond to the white spots in SEM images shown in Figure 7. Element mappings demonstrated that the spots are rich in Si and oxygen content and poor in Na and Al content. The spherical structures imply that they were liquid at elevated temperatures corresponding to a silica-rich glass formed during the anode backing process. Point analysis confirmed that the Na and Al content in the silica droplets was less than 1 at% and 5 at%, respectively. Silica droplets solidify when the flue wall cools down, which seems to serve as nucleation and deposition surface for pyrolytic carbon to grow during the next firing cycle. Different phases observed in the sample were not necessarily formed at the same time.

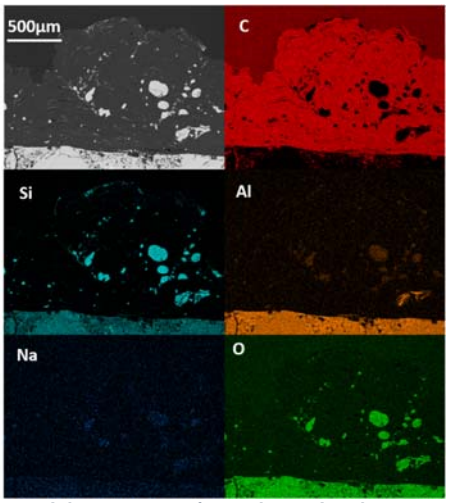

Figure 7. Backscatter SEM image and element mapping of C, Si, Al, Na and O. The spots on refractory surface were silica.

Silica spots were also observed in the vicinity of the refractory surface. The electron image and element mapping of C, Si, Al, S and O are presented in Figure 8. The formation of the silica phase is proposed to contribute both to the formation of carbon build-up layer and the degradation of the refractory materials. The mechanism for transporting silicon to the deposition sites, where pyrolytic carbon is formed, needs further studies.

Figure 9 shows an electron image of mullite grains together with element mappings. A Si depleted region along the mullite grain surface is evident in the Si element mapping, which indicates that the mullite grain has been attacked with loss of Si. The lost Si from mullite grains is suggested to contribute to the formation of silica droplets in the carbon build-up layer. Carbon deposition on pore surfaces was also evident in the C element mapping. Gaseous degradation of the mullite is proposed to be the underlying reason, which will be discussed later.

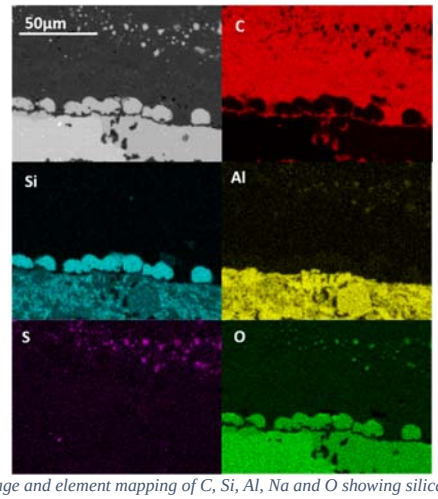

Figure 8. Backscatter SEM image and element mapping of C, Si, Al, Na and O showing silica spots on the refractory surface

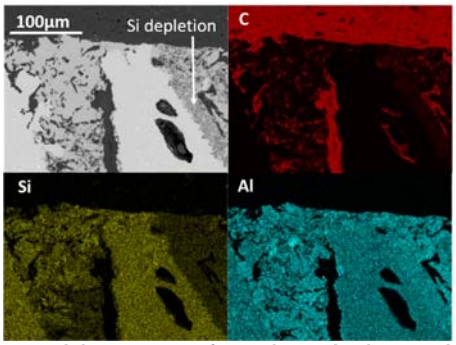

Figure 9. Backscatter SEM image and element mapping of C, Si, Al, Na and O showing Si depletion region on the mullite grain surface

A cylindrical sample was drill from the spent flue wall brick with a layer of carbon build-up attached to the refractory. The sample was analysed using X-ray CT scanner to see the microstructure evolution in the interior of the material. Images of CT scan are shown in Figure 10 where orthogonal views of the xz plane is shown in a) while the xy plane is shown in b) and c). The brighter the colour in the figures are the heavier are the element phases. The darker colour corresponding to less heavy element phases is explicitly carbon in this sample. Delamination was observed at the refractory interface probably due to the thermal history. Many white sports were found in the carbon build-up layer, which were silica droplets according to the previously mentioned SEM/EDS analysis. At the exact interface, in the gaps, white needles/rods phases were observed as shown in Figure 10 b). Cylindrical sample was carefully broken along the interface for further SEM/EDS analysis to investigate the phase composition of the needles/rods.

Figure 11 a) shows a rich rods area corresponding to the white needles/rods in the CT scans. The surface of the rods contains mainly carbon. Figure 11 b) and c) display the broken particle with the rods. A core-shell structure is evident with a solid core wrapped in shell layered pyrolytic carbon. The hexagonal cores are clearly shown in Figure 11d).

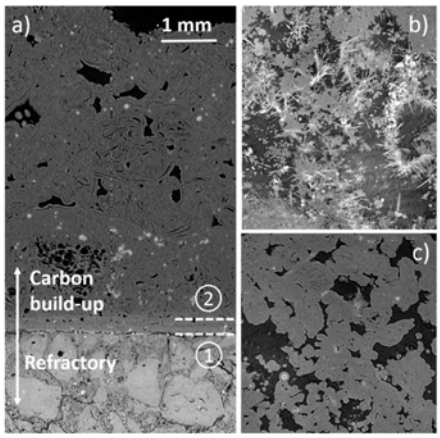

Figure 10. X-ray computed tomography images of carbon build-up at the refractory interface. a) xz cross-section, b) and c) xy cross-section along line number 1 and 2 in a). Needles or rods were found in the gaps as shown in b).

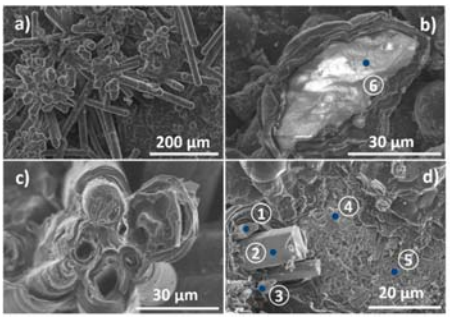

Figure 11. SEM images of rods at the refractory and carbon build-up interface. a) bunch of rods; b)-c) broken particle and rods with layered pyrolytic carbon shell and solid cores; and d) hexagonal core structure. Number 1-6 are positions for point analysis.

Point analysis was performed to check the elemental compositions of each phase. Results of points 1-6, highlighted in Figure 11, are summarized in Table 1. The hexagonal rods (point 1-2) and the smaller grains at the background (point 4-5) had significantly higher Al content compared to the previously mentioned silica droplets away from the refractory surface. They are close to the mullite composition as listed at the bottom of Table 1. The irregular big grain (point 6) and the small droplet (point 3) are silica phases. The sample used for illustration has fractured surface to better display the morphology. Some uncertainties in the element analysis must be expected due to the sample topography.

Table 1. Element compositions of point 1-6 in Figure 11 from EDS point analysis (unit in at%). Two mullite compositions are also include for comparison

	Al	Si	Na	O
Point 1	34.1	8.4	0.5	56.7
Point 2	32.1	9.2	0.4	58.1
Point 3	0.5	34.2	0.1	60.2
Point 4	29.4	10.5	0.2	59.1
Point 5	32.3	10.4	0.1	56.2
Point 6	2.7	31.0	0.3	66.1
Mullite ($3Al_2O_3{\cdot}2SiO_2$)	28.6	9.5	/	61.9
Mullite ($2Al_2O_3{\cdot}SiO_2$)	30.8	7.8	/	61.6

3. Discussion

3.1 Formation Mechanisms of Carbon Build-Up

The formation of pyrolytic carbon, resulting from hydrocarbon cracking and subsequent nucleation and growth on the hot surfaces at the flue wall, play an important role in the formation of the carbon build-up layer on flue wall surfaces. The process of pyrolytic carbon deposition can be described as CVD (chemical vapour deposition) on a hot substrate or CVI (chemical vapour infiltration) on porous materials [7, 9, 10].

Hydrocarbon volatiles are released from the pitch during heating of the green anodes. Once released, the volatiles are sucked into the flue cavity through open slits and porosity in the flue wall. The burning of the volatiles from the pitch contributes around 40 % to 50 % of the total furnace energy input. A reduced pressure in the flue is maintained for sucking the volatiles [4] out of the pits. This also gives sufficient mass flux for the deposition of pyrolytic carbon by the CVI route. Sufficient mass flux is necessary for yielding pyrolytic carbon instead of carbon black, which normally nucleates in the gas phase and not on a hot surface [7]. The deposited pyrolytic carbon then gradually fills up the voids between the flue wall and packing coke, as well as the voids between packing coke particles. As a result, the packing coke particles fuse together and bind to the refractory surface. In the course of time, a hard carbon build-up layer accumulates on the flue walls. Volatiles also infiltrate the refractory through pores and cracks leading to the observed pyrolytic carbon deposition in pores. A schematic drawing illustrating the build-up formation mechanisms is shown in Figure 12. In addition to the packing coke particles, solidified silica droplets and the mullite like rods at the refractory interface are also important sources for pyrolytic carbon deposition and subsequent growth. Na seems to have no or limited contribution in the formation of build-up.

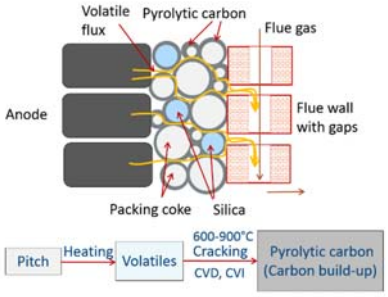

Figure 12. Schematic drawing illustrating the carbon build-up mechanisms. Figure not in scale.

3.2 Transport of Silicon to the Carbon Build-Up Layer

Silica particles, covered by layered pyrolytic carbon, were found not only at the refractory interface but also in the carbon build-up layer away from the refractory. These silica particles are produced in-situ during the anode backing process. The transport of silicon to the reaction site is important to understand. Silicon monoxide gas (SiO) is proposed to be the silicon carrier. Several reactions may contribute to SiO (g) formation.

Cristobalite in the refractory wall is unstable in contact with carbon at high temperatures. Cristobalite can be converted into volatile SiO (g) by Reaction 1 with a negative Gibbs free energy of -643 kJ/mol. The process is spontaneous at standard state. Moreover, the "silicon depletion region" on a mullite particle surface, as shown in Figure 9, strongly suggests a mullite decomposition reaction. Mullite decomposition may occur in a CO or H_2 atmosphere or in contact with carbon at certain oxygen partial pressure [11, 12]. The possible reactions are summarized in Table 2, as Reaction 2-4, with the corresponding standard Gibbs energies.

Table 2. Possible reactions and the corresponding standard Gibbs energies

	$\Delta G(1300°C)$ $[kJ/mol]$	
$SiO_2 + C = CO(g) + SiO(g)$	-643.0	(1)
$3Al_2O_3 \cdot 2SiO_2(s) + 2CO(g) \leftrightarrow 3Al_2O_3(s) + 2SiO(g) + 2CO_2(g)$	+49.3	(2)
$3Al_2O_3 \cdot 2SiO_2(s) + 2C \leftrightarrow 3Al_2O_3(s) + 2SiO(g) + 2CO\ (g)$	+324.5	(3)
$3Al_2O_3 \cdot 2SiO_2(s) + 2H_2(g) \leftrightarrow 3Al_2O_3(s) + 2SiO(g) + 2H_2O\ (g)$	+21.9	(4)

Mullite decomposition Reactions (2-4) are energetically unfavoured in the standard states. By lowering the partial pressure of SiO (g), however, the reactions will shift to the right hand sides and cause decompostion of mullite. The large pressure drop in the open baking furnace, sucking the gaseous products from the reaction site into the flue cavity, will contribute to a low SiO pressure and thereby promote the mullite decomposition. A predominance diagram of Al-Si-C-O system at 1300 °C is shown in Figure 13. The diagram presents the stable field of each phase as a function of chemical potentials. The partial pressure of SiO (g) was fixed at 1×10^{-8} atm in the calculation. Under this situation, mullite is unstable when the oxygen partial pressure is lower than $1\times10^{-11.4}$ atm. Corundum and SiO (g) will be the stable phases at oxygen partial pressure in the region of 1×10^{-26} to $1\times10^{-11.4}$ atm.

Deleted: Figure 13

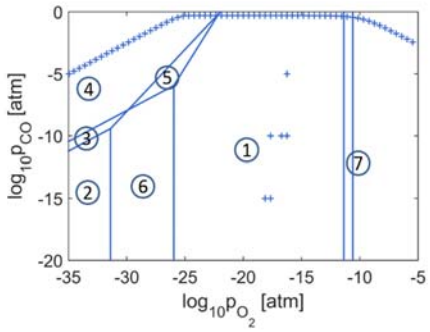

Figure 13. Predominant phase diagram of Al-Si-C-O system at 1300 °C. 0.3333 < Si/(Si+Al) <0.5, $p_{SiO2} = 1\times10^{-8}$ atm. 1. Al_2O_3-SiO(g); 2. Al(l)-Si(s); 3. Al(l)-SiC(s); 4. Al_4C_3(s)+SiC(s); 5. Al_3C_4(s) + SiO(g); 6. Al(l)-SiO(g); 7. $2Al_2O_3{\cdot}2SiO_2$; and "+" denotes 1.0 atm isobar. Calculated using FactSage [6]

Corundum grains were not detected by SEM, instead, mullite-like rods wrapped in laminar pyrolytic carbon were found at the vicinity of refractory interface. This might be the so-called secondary mullite, where corundum recombined with SiO (g) and formed mullite grains again. This phenomenon is also reported in other process [11]. Mullite-like rods are only found at the refractory interface. Re-oxidation of the volatile SiO (g) occurs upon cooling. Silica droplets solidify at the fresh build-up surface and severe as pyrolytic carbon nucleation sites in the next heating section. Hence, over time, silica droplets will be observed all over the entire carbon build-up layer.

3.3 Parameters influencing the carbon build-up formation

Large pressure drop between the anode pit and flue cavity is necessary to give sufficient mass flux for pyrolytic carbon to form through a CVI route. This large pressure drop is the nature of the open top baking furnace, but not an issue in a closed type furnace, therefore the formation of pyrolytic carbon in a closed furnace is not likely. The mechanisms for carbon build-up in a closed type furnace will be different and the corresponding results will be reported elsewhere.

Packing coke particle size distribution is another parameter influencing the carbon build-up formation. Fines or smaller particles partially fill the voids between larger particles and the space between the coarser coke particles and the flue wall, as illustrated in Figure 12. The remaining free space will be significantly smaller compared to the case with only large particles, while the surface area will be much larger. The increased surface area will increase the driving force of fusing. Therefore, coke particles with fines or small particles will be easier to fuse together and fixe to the flue wall to form a solid attached build-up layer when all the free spaces are filled up by carbon. Logically, the process will be much faster when the packing coke consists of a finer fraction due to the less free space. Large surface area, associated with fines, also provides more nucleation sites for pyrolytic carbon deposition. Removing the fines in the packing cokes is recommended for reducing the carbon build-up.

4. Conclusion

The formation of pyrolytic carbon, resulting from hydrocarbon cracking and subsequent nucleation and growth on hot surfaces, plays an important role on the formation of carbon build-up layer on flue wall surfaces. The hot surfaces for pyrolitic carbon deposition can be packing coke particles, solidified silica droplets or mullite-like rods. The mullite-like rods were mostly like secondary mullite found only at the refractory interface, while the silica particles were found spread all over carbon build-up layer. SiO (g) is the most likely "silicon" carrier, resulting from the decomposition of mullite grains under the exposure to CO (g) or H_2 (g). The pressure drop towards the flue wall removes SiO (g) from reaction site and promotes mullite decomposition. The pressure drop also provides enough mass flux of volatiles, which is necessary for pyrolytic carbon formation. Fines in the packing coke also enhance the formation of carbon build-up.

Acknowledgement

The present work was carried out in the project "Reactivity of Carbon and Refractory Materials used in Metals Production Technology" (CARMA), financed by the Research Council of Norway, Hydro Aluminium, Alcoa Norway, Skamol, and Elkem Carbon. Permission to publish the results is gratefully acknowledgement.

Reference

1. Tiba, P.R.T., et al., *Systemic analysis of flue wall bricks used on anode baking furnaces.* Light Metals, 2010: p. 1015-1019.
2. Prigent, P., et al., *The effect of the addition of fine andalusite particles in refractory bricks on gaseous corrosion.* JOM, 2008. **60**(5): p. 58-63.
3. Brunk, F., *Corrosion and Behaviour of Fireclay Bricks Used in the Flues of Open Anode Baking Furnaces.* Light Metals, 1995: p. 641-646.
4. Keller, F. and P.O. Sulger, *Anode Baking*. 2nd ed. 2008, Sierre, Switzerland: R&D Carbon Ltd.
5. Brandvik, T., Z. Wang, and T. Grande, *Investigations of spent refractory lining in an anode baking furnace.* Light Metals, 2017.
6. Bale, C.W., et al., *FactSage thermochemical software and databases.* Calphad-computer Coupling of Phase Diagrams and Thermochemistry, 2002. **26**(2): p. 189-228.
7. Bourrat, X., et al., *Low temperature pyrocarbons: a review.* Journal of the Brazilian Chemical Society, 2006. **17**: p. 1090-1095.
8. Guellali, M., et al., *Textures of pyrolytic carbon formed in the chemical vapor infiltration of capillaries.* Carbon, 2003. **41**(1): p. 97-104.
9. Vignoles, G.L., et al., *CVD and CVI of pyrocarbon from various precursors.* Surface and Coatings Technology, 2004. **188–189**: p. 241-249.
10. Delhaes, P., *Chemical vapor deposition and infiltration processes of carbon materials.* Carbon, 2002. **40**(5): p. 641-657.
11. Wright, R.E. and H.I. Wolff, *Refractory Problems in Production of Hydrogen by Pyrolysis Natural Gas.* Journal of the American Ceramic Society, 1948. **31**(2): p. 31-38.
12. Davis, R.F., I.A. Aksay, and J.A. Pask, *Decomposition of Mullite.* Journal of the American Ceramic Society, 1972. **55**(2): p. 98-101.

Figure captions:

Figure 14. Carbon build-up sample (left top), interface sample (left bottom), and a schematic drawing (right) partly showing an open anode baking furnace structure which is relevant to the present work. 1 - hollow flue wall bricks, 2 - gaps in flue walls to exhaust the volatiles, 3 – packing coke, 4 – green anodes, and 5 – carbon build-up on flue wall surface. Figure only for illustration and not in scale.

Figure 15. SEM images of carbon build-up. a) cross-section, and b) fracture surface. 1. packing coke particle; 2. layered carbon structure growing on top of the coke particle and white spots; 3. white silica spots

Figure 16. Polarized light micrographs of cross-section of carbon build-up. a) spherical laminar structure with cleavage planes, and b) Ribbon-like structure surrounding a needle coke particle. The two figures have the same magnification

Figure 17. Polarized light micrographs of cross-section of carbon build-up. a) – b) position towards flue wall, and c) - d) position towards packing coke

Figure 18. XRD diffractograms for carbon build-up and pristine packing coke

Figure 19. Polarized light micrographs of cross-section of carbon build-up and refractory interface

Figure 20. Backscatter SEM image and element mapping of C, Si, Al, Na and O. The spots on refractory surface were silica.

Figure 21. Backscatter SEM image and element mapping of C, Si, Al, Na and O showing silica spots on the refractory surface

Figure 22. Backscatter SEM image and element mapping of C, Si, Al, Na and O showing Si depletion region on the mullite grain surface

Figure 23. X-ray computed tomography images of carbon build-up at the refractory interface. a) xz cross-section, b) and c) xy cross-section along line number 1 and 2 in a). Needles or rods were found in the gaps as shown in b).

Figure 24. SEM images of rods at the refractory and carbon build-up interface. a) bunch of rods; b)-c) broken particle and rods with layered pyrolytic carbon shell and solid cores; and d) hexagonal core structure. Number 1-6 are positions for point analysis.

Figure 25. Schematic drawing illustrating the carbon build-up mechanisms. Figure not in scale.

Figure 26. Predominant phase diagram of Al-Si-C-O system at 1300 °C. $0.3333 < Si/(Si+Al) < 0.5$, $p_{SiO2} = 1\times10^{-8}$ atm. 1. Al_2O_3-SiO(g); 2. Al(l)-Si(s); 3. Al(l)-SiC(s); 4. Al_4C_3(s)+SiC(s); 5. Al_3C_4(s) + SiO(g); 6. Al(l)-SiO(g); 7. $2Al_2O_3{\cdot}2SiO_2$; and "+" denotes 1.0 atm isobar. Calculated using FactSage [6].

Deleted: 1

Deleted: 2

Deleted: 3

Deleted: 4

Deleted: 5

Deleted: 6

Deleted: 7

Deleted: 8

Deleted: 9

Deleted: 10

Deleted: 11

Deleted: 12

Deleted: 13